ELSEVIER

Contents lists available at ScienceDirect

Electric Power Systems Research

journal homepage: www.elsevier.com/locate/epsr



Toward large-scale aircraft-based measurements of energetic radiation from thunderstorms and lightning

Istvan Kereszy ^{a,*}, Vladimir A. Rakov ^a, Attila Gulyas ^b, Ziqin Ding ^a, Teruaki Enoto ^c, Yuuki Wada ^d, Listz Araújo ^e, Miguel Guimarães ^e

- ^a Department of Electrical and Computer Engineering, University of Florida, Gainesville, USA
- ^b Nuclear Security Department, Centre for Energy Research, Budapest, Hungary
- ^c Department of Astronomy, Faculty of Science, Kyoto University, Kyoto, Japan
- ^d Department of Electric, Electronic, and Infocommunications Engineering, Osaka University, Osaka, Japan
- e Laboratory of Electromagnetic Transients (LabTEM), Federal Center for Technological Education of Minas Gerais (CEFET-MG), Belo Horizonte, Brazil

ARTICLE INFO

Keywords: Thunderstorms Lightning Energetic radiation TGFs TGEs Aircraft measurements Laboratory testing

ABSTRACT

Thunderstorm and lightning related energetic radiation can generally be categorized as (1) leader X-rays, (2) Terrestrial Gamma-ray Flashes (TGFs), or (3) Thunderstorm Ground Enhancements (TGEs). TGFs are usually recorded from satellites, and, on some occasions, they have been recorded from the ground, but only a few attempts have been made to measure TGFs from aircraft. Thunderstorm Ground Enhancements (TGEs) are much longer duration than TGFs, and they are recorded at ground level. Energetic radiation associated with thunderstorms and lightning is a relatively recently recognized hazard. It can have possible adverse effects on commercial and general aviation avionics, thus an experimental understanding of the impulsive and prolonged radiation enhancements onboard aircraft is essential (Eack et al., 1996). In this paper, we present artificial TGFs and TGEs, which were acquired in the lab with a compact CsI scintillator detector, along with commercial and general aviation aircraft-based measurements to assess the feasibility of a large-scale aircraft-based study. Our preliminary results include 180 h of aircraft-based measurements, the longest aircraft-based TGF search to date, and show that the detector hardware, installation protocol, processing software, and search algorithm can be used for a large-scale study of energetic radiation from thunderstorms and lightning.

1. Introduction

Terrestrial Gamma-ray Flashes (TGFs) with individual pulse energies ranging from 80 keV up to 40 MeV or more have mostly been observed from orbiting satellites and only a handful of events were recorded at ground level [1–3]. Thunderstorm Ground Enhancements (TGEs) are much longer duration than TGFs, and they are recorded from the ground [4–8]. Satellite-based observations of TGFs include those obtained in the Burst and Transient Source Experiment (BATSE) aboard NASA's Compton Gamma-ray Observatory (CGRO) [9,10], with the Reuven Ramaty High Energy Spectroscopic Imager (RHESSI) [11,12], a NASA small satellite, the Gamma-ray Burst Monitor (GBM) on NASA's satellite-based Fermi Gamma-ray Space Telescope (Fermi) [13–15], and the Italian satellite AGILE [16–18]. In the datasets obtained by these satellites, TGFs mostly happened in tropical and coastal regions, as opposed to occurring inland or over oceans [19].

One difficulty in the interpretation of satellite observations of TGFs is the lack of detailed information on lightning processes (besides the often-used locations from the World Wide Lightning Location Network (WWLLN)) that potentially cause TGFs. Such information is available at ground-based lightning observation stations, but those, with a few exceptions in Florida, Utah, and Japan, are not equipped with adequate TGF detectors. Another inherent deficiency of satellite records is the timing uncertainty of a few milliseconds due to the large field of view of onboard detectors and unknown long propagation paths from thunderstorms to the detectors. Aircraft-based measurements are much more informative as they are closer to the source (expected to be at cloud altitudes) than either ground-based or satellite-based detectors. Fig. 1 shows a summary of the various approaches.

Energetic particles can interact with commercial and general aviation avionics with possible negative impacts; thus an experimental understanding of the impulsive and prolonged radiation enhancements

E-mail address: ikereszy@ufl.edu (I. Kereszy).

 $^{^{\}ast}$ Corresponding author.

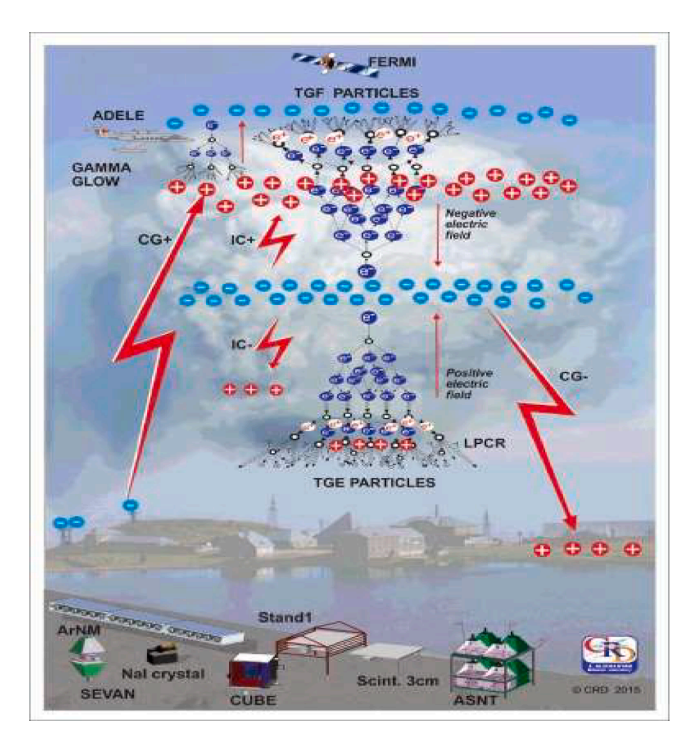


Fig. 1. Schematic illustration of ground-based and aircraft (ADELE) observations of gamma-ray glows (Thunderstorm Ground Enhancements or TGEs) and satellite (FERMI) observations of TGFs. Adapted from Chilingarian et al. [16].

onboard aircraft is essential [20-22]. While there are several publications about the measurement of TGFs from aircraft and balloons [23-25], they are limited in terms of duration and spatial extent, as well as temporal and spectral resolution, and they never fully addressed the question of in-flight radiation. Such aircraft-based measurement campaigns include the In-Flight Lightning Damage Assessment System (ILDAS) which used an Airbus A340 test aircraft that intentionally flew near thunderstorms. This experiment detected gamma-ray enhancements 20 times higher than the background levels that lasted between 20 and 30 s [26,27]. Similarly, the Airborne Detector for Energetic Lightning Emissions (ADELE) used a Gulfstream V jet near thunderstorms and recorded both a TGF and gamma-ray glows [28,29]. These papers serve as valuable evidence for the value of aircraft-based TGF and gamma-ray glow search. There is a need for a more systematic study, but it has not been done thus far [19,26-31]. We propose to use a set of innovative, small, and lightweight radiation detectors with good spectral resolution to explore diverse conditions and radiation sources, as well as collect potentially far more data than was possible before. The most thorough aircraft based TGF measurements to date include the ILDAS and ADELE experiments, but they have been carried out by individual aircraft over only 37 flight hours [26,28].

We performed the calibration of the prototype instrument, developed a self-contained battery-based power supply, and created the inflight data management protocols. These were tested and refined during our trial run that included 16 flights over 180 h of flight data (vs. 37 h in previous studies), and several different aircraft types. This approach is novel, because it does not require dedicated scientific aircraft that are costly to rent and operate. Instead, it relies on a new method of conducting extensive measurements onboard commercial and general aviation aircraft during their routine operations. This mission is unique and improves on previous studies, as it enables measurements during real-world flight scenarios and significantly reduces costs. The preliminary results support the need for a larger-scale study that builds on our current results which demonstrated the technical and scientific feasibility of systematically searching for TGFs and TGEs using aircraft.

Historically, there has been a disciplinary divide between those who

study the incidence and atmospheric transport properties of galactic cosmic rays and solar energetic particles, and those who conduct research on lightning and TGFs. During our research we aimed to combine the lightning and TGF related measurements that we conduct at the Lightning Observatory in Gainesville (LOG) and the astroparticle physics and cosmic-ray related calculations to result in location specific cosmic radiation, lightning, and TGF models. In a combination of theoretical calculations and experimental measurements we were able to calibrate the instruments, redesign them for flight, calculate altitude dependent baseline levels, develop aircraft-based X-ray measurement routines, and write TLE and TGF search algorithms. This is key for a holistic understanding of cosmic rays, lightning, TGFs, and the connection between space and terrestrial weather systems. Specifically, the source of the initial relativistic electrons, which lead to the avalanche multiplication of electrons that result in TGFs and may play an important role in lightning initiation, is still not known. Cosmic rays may act as the necessary high energy seed particles [19]. Finally, our modeling work can serve as the basis for the addition of thunderstorm related radiation to the Federal Aviation Administration's (FAA) CARI-7 framework for monitoring in-flight radiation doses for passengers and crew, in order to lower the energetic radiation risks in flight for all of us.

The objective of the present study was to better understand the energetic radiation environment encountered by commercial and general-aviation (GA) aircraft and its potential hazard for passengers and crew members. Extensive calibration measurements were conducted using eight different radioactive isotopes to test the portable gamma-ray detector photopeak response. Dynamic track measurements were completed to test how the detector will respond to both slow and fast impulses, and large intensity sources were used to test detector performance when it is saturated. We found that the detector had a photopeak measurement uncertainty of ± 20 keV, and that it had a memory overflow problem when it reached saturation. We used high-intensity short pulses to test how the detector would respond to Terrestrial Gamma-ray Flash (TGF) events and what detector response would be triggered by Thunderstorm Ground Enhancements (TGEs) that are much longer than TGFs.

2. Methods and technical approach

Previous studies considered the average flux of cosmic-ray primary particles and their anisotropy at various energies [32–34] confirming that cosmic-ray arrival is a stochastic process with large locational dependence due to geomagnetic shielding. Both satellite based and ground based cosmic-ray telescopes tend to not fully grasp directionality and location dependence. On the other hand, our aircraft-based detectors serve as moving pixels that detect cosmic-rays and accurately represent the conditions at that specific location and altitude.

The new GOES-R series of geostationary satellites provide real time publicly accessible data on the heliospheric magnetic field and energetic particle flux, including an expanded variety of ions, which allows a more complete analysis of solar cosmic radiation and galactic cosmic radiation. The National Oceanic and Atmospheric Administration's (NOAA) Space Weather Prediction Center has already started to use these data for the creation of advance warning systems for aircraft that calculate the flux of energetic primary and secondary particles at various altitudes and locations. Currently, FAA's CARI-7 radiation monitoring system uses the aforementioned satellite data through the program Maps of Ionizing Radiation in the Atmosphere (MIRA).

2.1. Aircraft-based TGF and TGE search

Our study includes a systematic aircraft-based TGF search, so it can improve the models to accurately forecast radiation at given locations, altitudes, and times with a view toward the lowering of energetic radiation risks in flight. All measurements presented in this paper were performed under fair-weather conditions. A small self-contained Cesium



Fig. 2. Prototype Cesium Iodide scintillator-based Gamma-ray detector that has been deployed on commercial aircraft. The current data acquisition system uses time bins of $100~\mu s$, and records photons from 300~keV to 10~MeV in five energy bins. Initial detector design and image provided by the University of Kyoto.

Iodide scintillator-based Gamma-ray detector has been placed on each aircraft participating in the study. This detector was used for all of the data collection in the present study. For the aircraft-based TGF and TGE search, the general method was similar to previous aircraft-based campaigns, such that the background radiation was determined and then the statistical significance of gamma-ray glows and TGF radiation peaks were calculated [26-29]. However, it is important to note that in this study, the data analysis included measurements taken during real commercial and general aviation flights, thus the flight altitudes and background radiation levels were constantly changing. Extensive lab-based calibration was conducted, as described in Section 2.2, to determine the response of the detector to radiation of varying intensity and spectral hardness. Here the same approach was taken as in previous studies, whereby isotopes with known emission lines were used to calibrate the energy response of the detector, and pulsated fields were used to test the temporal response [35]. We used the detector on various routes, but in the future we will especially focus on routes that fly close to the equator due to higher numbers of TGFs there, and close to the poles due to increased exposure to cosmic rays.

Terrestrial Gamma-ray Flashes (TGFs), known to originate from thunderstorms, are the highest-energy natural photon fluxes on Earth. While the FAA advises pilots to avoid flying through or close to thunderclouds, each commercial aircraft is struck by lightning (usually during take-off or landing) on average once a year [36]. According to Dwyer et al. [30], the radiation dose received by passengers and crew in flight, when airborne vehicles are close to a TGF event, could reach a biologically harmful level (0.1 Sv) in less than 1 ms. The mechanism of TGFs remains the subject of debate [37,38]. To shed more light on the nature of TGFs, we have conducted an aircraft-based X-ray and Gamma-ray measurement campaign. Systematic radiation measurements were performed onboard commercial aircraft using a prototype Cesium Iodide scintillator-based Gamma-ray detector (Fig. 2). The data acquisition system had time bins of 100 µs and recorded photons from 300 keV to 10 MeV in five energy bins, and the sixth energy bin was reserved for all photons with energies above 10 MeV. Preliminary results based on several months of systematic observation are presented below. We found that in certain energy bins the radiation levels at cruising altitudes are a factor of 160 higher than the levels measured on the ground with the same instrument, which we used to develop both TGE and TGF search algorithms with a redefined baseline radiation levels.

Table 1List of radioactive isotopes used for calibration, along with their gamma photopeak energies and detector channel readouts.

Isotope	Gamma energy [keV]	Channel	
Co-57	122	25	
Cs-137	662	64	
Mn-54	834	90	
Co-60	1173	123	
Na-22	1274	138	
Co-60	1332	142	
Eu-152	1408	153	
Tl-208	2614	284	

Furthermore, it permitted us to search for the presence of gamma-ray glows at various altitudes.

2.2. Instrumentation and its lab-based testing

A Cesium Iodide scintillator-based Gamma-ray detector was extensively tested in the laboratory and deployed on both general aviation and commercial aircraft. We calibrated the instrument using 8 different types of isotopes (Co-57, Cs-137, Co-60, K-40, Eu-152, Mn-54, Na-22, Tl-208) over a wide energy range (122 keV to 2614 keV). This covers the energy range practically attainable with widely accessible radioactive isotopes and this is the range that was used for the calibration to comply with the single photon calibration methodology. Due to the pileup effect the energies of individual photons are linearly added up within a single time window, so energies within the entire measurement energy range were observed, as noted in Section 3.5. This gave us insights into the response of the detector at various photon energy levels, and we were able to link gamma photopeak energy value to detector channel readouts. Linear and quadratic fits were used to find the equation that best approximates the observed data. Table 1 shows the isotopes used, their photopeak energies, and the channel that they triggered in the detector.

Calibration was performed during the summer of 2021 at the Nuclear Security Department of the Hungarian Centre for Energy Research (EK), where we performed various studies to better understand the temporal and spectral responses of the detector. The following five detector performance characteristics were studied:

- 1. Photopeak energy response
- 2. Directional dependence
- 3. Temporal resolution (Artificial TGE)
- 4. Spectrum consistency at varying intensities
- 5. Response to short impulses (Artificial TGF)

Directional dependence of the crystal, dose rate - count rate - channel interconnection and saturation behavior were tested at calibrated doserate points in stationary radiation field up to a thousand times the value of the natural background radiation. Despite the elongated crystal shape (5 cm x 5 cm x 15 cm), there is no significant directional dependence. We developed a TGE search algorithm which plots and detects TGE events and separates them from background noise. We tested the algorithm both on the ground during laboratory experiments and in-flight.

3. Data collection and analysis

In order to calibrate the CsI scintillator-based gamma-ray detector used at LOG, we performed a series of tests using radioactive isotopes with known emission lines.

3.1. Photopeak analysis

These measurements allowed us to calibrate the a, b, and c factors used in the second-degree polynomial

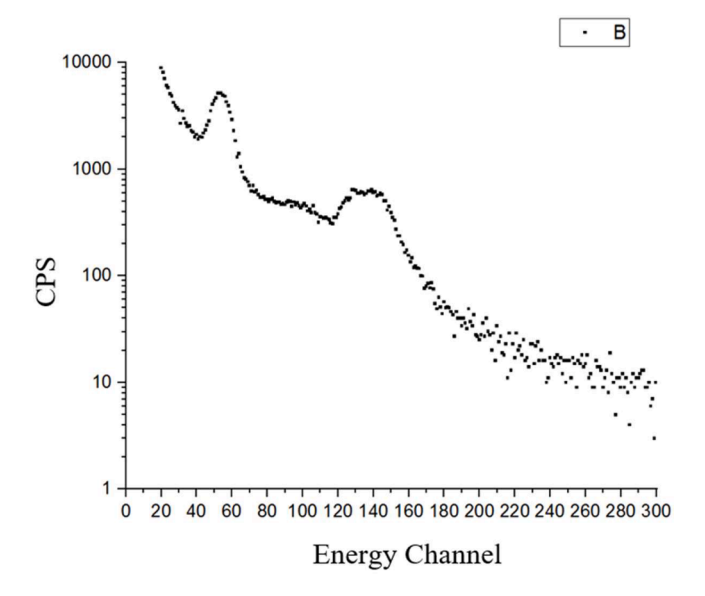


Fig. 3. Measured X-ray count per second rate (CPS) as a function of detector energy channel (ch) for part of the energy spectrum (channels 20–200).

$$a*ch^2 + b*ch + c \tag{1}$$

to accurately relate the channel number (ch) to photon energy in keV. We were also able to determine the maximum precision of the detector by fitting a Gaussian curve to the photon spectrum reported by the device. In addition, we tested the time response of the detector, the maximum flux that it can accurately report, as well as the detector response above saturation level. In Figs. 3 and 4 we can see the photopeak analysis for Na-22.

We performed the linear, quadratic, and cubic fitting for all 8 isotopes. The cubic term is negligible and we present the other coefficients in Table 2.

It is clear from the above that the quadratic term makes a very small contribution, even for the largest channel numbers (maximum channel number is 1019), so that a linear approximation is sufficient, especially for the lower energy levels. We now drop quadratic terms in both Dr.

Enoto's and our equations and compare just the b-values. In our study, the largest b value is associated with the quadratic fit for all 8 isotopes (b=10.62), and the smallest b value is associated with the quadratic fit for the 7 isotopes, excluding Co-57 (b=8.18, 23% smaller). The value of b=8.4787 provided by Dr. Enoto is within this range. There is considerable difference in the constant term (c) of the polynomial equation, which ranges from -89.52 to 113.38. The c values are positive for the cases where the fit was achieved for the seven isotopes excluding Co-57 and negative when all eight isotopes were used. The low photopeak energy of Co-57 (130 keV) has a large effect on the c values since the c values are most relevant near the lowest energy channel readouts (the lowest channel value is 20). It is important to note that the detector channel readout is related to the energy deposited in the detector and not to the total energy of the X-ray or Gamma-ray. This means that there is an inherent uncertainty in measuring X-ray energies with scintillators.

3.2. Distance dependence and saturation

We located the crystal center along the three axes and positioned the detector such that in each configuration these markings would line up with the axis of the gamma-ray beam (Fig. 5). A 46 MBq Cs-137 source was used throughout the distance measurements.

The source was fixed and the detector was placed on a trolley that moved along a track parallel to the axis of the gamma-ray beam. In addition to the relative distance between the source and the detector, the orientation of the detector was also switched between the long axis and

Table 2Summary of the equation types and constants (a,b,c) used to convert detector energy channel readouts to energy in keV.

	Original quadratic equation []	Linear fit for all 8 isotopes	Quadratic fit for all 8 isotopes	Linear fit for the 7 isotopes excluding Co-57	Quadratic fit for the 7 isotopes, excluding Co-57
Equation type a b	$a \cdot ch^2 + b \cdot ch + c$ 0.0015 8.4787 -17.13	b·ch + c NA 9.36 -14.64	$a \cdot ch^2 + b \cdot ch + c -0.004$ 10.62 -89.52	<i>b</i> ⋅ <i>ch</i> + <i>c</i> NA 8.97 54.72	$a \cdot ch^2 + b \cdot ch + c$ ch + c 0.0022 8.18 113.38

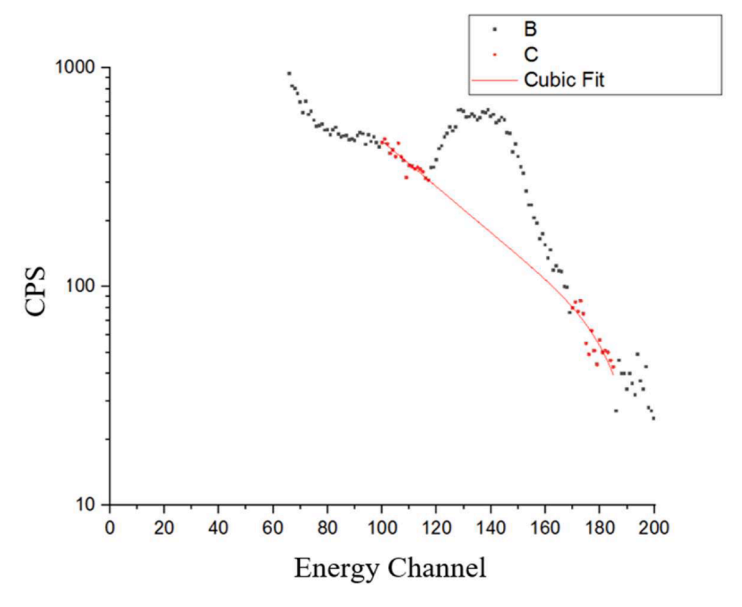


Fig. 4. Cubic fit for the Na-22 photopeak located near channel 138 (1274 keV). Contains datapoints both inside and outside the photopeak. The plot symbols labeled C (red circles) represent the points that lie outside the photopeak (these are the points used to calculate the baseline). The plot symbols labeled B (black squares) represent the points that are part of the photopeak calculations.

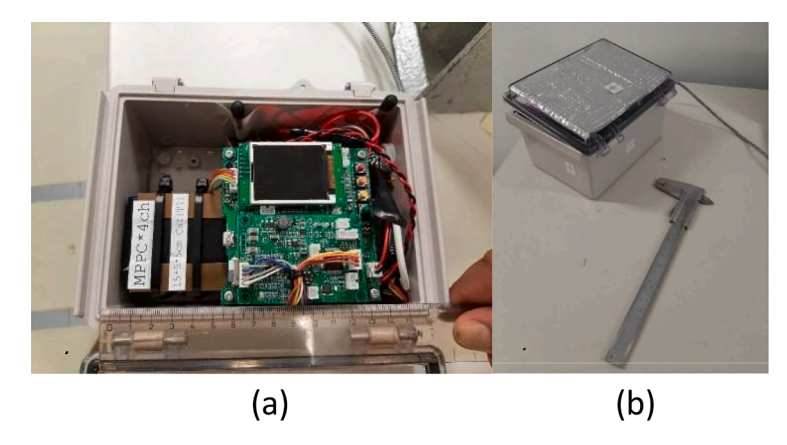


Fig. 5. Locating the crystal center along the three axes. The $15 \times 5 \times 5$ cm CsI scintillator is visible in (a). The outside of the detector was marked at the crystal centers (b).

Table 3Measured X-ray intensity (CPS) as a function of distance from Cs-137 source. The CPS values stabilize once the saturation level is reached.

Measurement number	Orientation	Distance (mm)	Intensity (CPS)		
Measurement 1	Long axis	4365	180		
Measurement 2	Short axis	4370	120		
Measurement 3	Long axis	4384	170		
Measurement 4	Short axis	4423	160		
Measurement 5	Long axis	2316	500		
Measurement 6	Short axis	2321	320		
Measurement 7	Long axis	1405	800		
Measurement 8	Short axis	1412	600		
Measurement 9	Long axis	678	1800		
Measurement 10	Short axis	678	1400		
Measurement 11	Long axis	325	2500		
Measurement 12	Short axis	325	2300		
Measurement 13	Long axis	225	2500		
Measurement 14	Short axis	225	2500		

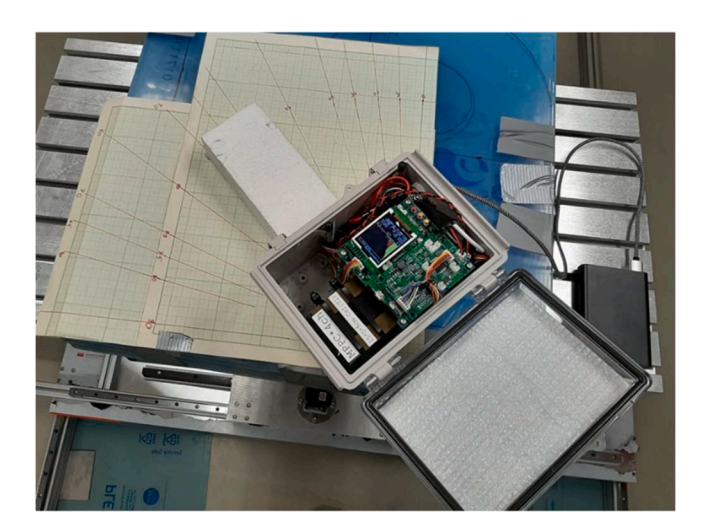


Fig. 6. The long axis of the gamma-ray detector was gradually reoriented relative to the gamma-ray beam.

short axis configurations after each measurement. As the separation between the detector and the source decreased, the intensity of the X-ray beam measured in counts per second (CPS) increased quadratically, until it reached saturation. The results are summarized in Table 3.

At 25,000 CPS the system became saturated and further decrease in the distance between the detector and the source did not result in CPS increases. This means that the detector is capable of distinguishing two

Table 4Measured X-ray intensity (CPS) as a function of detector orientation. The CPS values stabilize once the saturation level is reached.

Measurement number	Orientation (degrees)	Intensity (CPS)	
Measurement 1	0	2100	
Measurement 2	15	2100	
Measurement 3	30	2100	
Measurement 4	45	2000	
Measurement 5	60	1800	
Measurement 6	75	1500	
Measurement 7	90	1300	

pulses only if they are at least 40 μ s apart. The time resolution of the timestamps generated by the detector is 100 μ s, which means that when the detector is saturated, multiple pulses have the same timestamp.

As the orientation of the detector is changed from the long orientation to the short orientation, the configuration of the CsI scintillator changes relative to the gamma-ray beam. In the long orientation the cross-sectional area of the detector is $75~\rm cm^22$ ($15~\rm cm$ by $5~\rm cm$), while in the short configuration the cross-sectional area is $25~\rm cm^22$ ($5~\rm cm$ by $5~\rm cm$). On the other hand in the long orientation the photons entering the scintillator travel $5~\rm cm$ in the detector, while in the short orientation they travel $15~\rm cm$ so the portion of photons absorbed relative to the number that entered is expected to be higher.

3.3. Directional dependence of X-ray detections

The center of the CsI scintillator was placed at a distance of 3779 mm from the Cs-137 radiation source, and this distance remained unchanged throughout the experiment. The orientation of the longer axis the detector was slowly changed relative to the gamma-ray beam, 15° at a time, in order to map out the response of the detector to radiation coming from different directions (See Fig. 6). Measurements were taken for 60 s for each orientation and the results are presented in Table 4.

3.4. Artificial TGEs

In order to look for TGEs, we needed to create a dynamic testing environment where the radiation levels change on a slow timescale similar to the timescales of gamma-ray glows,tens of seconds to minutes as seen in ground-based studies. A dynamic track with a radiation source attached to an automated cart with an adjustable speed was used to test the response of the detector and the performance of the algorithm on various time scales.

A 46 MBq Cs-137 radiation source with a 662 keV photopeak was placed on the moving cart. The CsI gamma-ray detector was shielded with lead from the radiation source except for a small opening, such that



Fig. 7. Lead structure shielding the detector from the moving radiation source. The small 3 cm by 3 cm opening is shown by shining green laser light through it. This small opening allows the gamma-ray beam to pass without shielding when the moving radiation source is directly in front of the detector.

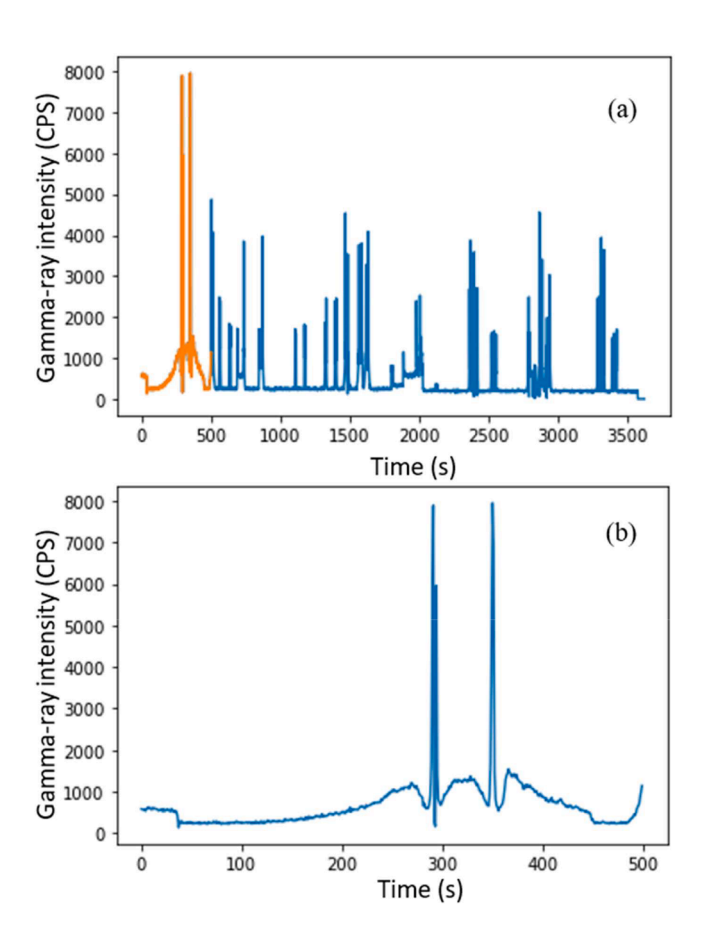


Fig. 8. (a) Interpretation of raw gamma-ray intensity data from artificial TGE measurements. The orange part is enlarged in (b) to show the gradual X-ray energy increase followed by the peaks, as the radiation source on the dynamic track passes the slits in the lead shielding.

the gamma-ray beam could only impact the detector for the brief period when the moving source was in front of the opening (see Fig. 7). Thus, depending on the speed of the source, enhancements of varying durations were produced and recorded by the detector.

These signals correspond to the dynamic track measurements, and the peaks occur when the gamma-ray source passes in front of the detector. As these are count-per-second (CPS) values integrated over one second, we expect that at slower speeds the enhancement will be larger as the time the radiation source spends in front of the 3 cm by 3 cm opening is longer. Thus, a larger number of photons can be deposited during the impulse. We can see in Fig. 8b how, despite the lead shielding, there is a visible gamma-ray enhancement from the 200 CPS level to the 1000 CPS level as the radiation source approaches the detector. This slow enhancement pattern that can last for tens of seconds or minutes is similar to a Terrestrial Ground Enhancement (TGE) and shows how the search algorithm that we used can be employed to effectively search for TGEs on the second, tens of second, and minute timescales.

Before the main peak, the CPS value briefly decreases and a similar pattern is visible on the other side of the gamma-ray intensity peak. This is due to the additional shielding provided by the lead when the radiation source is near and the number of reflected photons reaching the detector is reduced. The peak itself represents the period when the gamma-ray source passes in front of the 3 cm by 3 cm opening in the lead shielding. As the motion of the automated cart is symmetric (i.e. it moves from the starting position to the final position along a straight line with a constant speed, and it returns to the starting position with the same speed), we expect the gamma-ray emission signature to be symmetric as well. Indeed, this symmetry can be observed in the pulse displayed in Fig. 8b These experiments show how the detector responds to gamma-ray enhancements that last up to minutes, as well as how it records impulses with lengths ranging from three seconds (for the 1 cm/sec speed) down to approximately 100 ms (for the 220 cm/sec speed).

As the background radiation level changes with altitude, it is important to adjust the probabilities to account for altitude-dependent radiation baseline levels. First, we recalculated the probabilities for three altitudes:

- 1. Sea level
- 2. 1000 m (flight level for general aviation aircraft)
- 3. 10,000 m (flight level for commercial aircraft)

The Poisson distribution is used to determine the probability of having a certain number of photons reaching the detector within a given timeframe. With the expectation of λ events in a given time interval, the probability of k events in the same interval is:

$$P(k) = \frac{\lambda^k e^{-\lambda}}{k!} \tag{2}$$

Fig. 11 illustrate the expectation values for the number of photons of

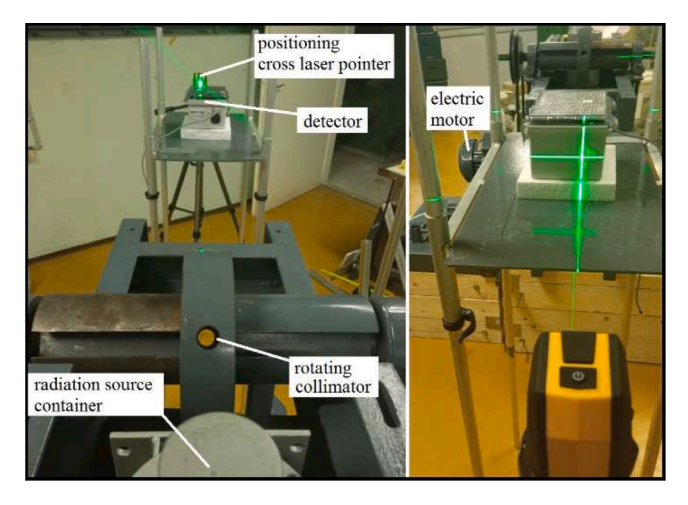


Fig. 9. (a) The full layout of the gamma-chopper experiment showing the radiation source, the 202 mm diameter rotating disk, the 22 mm diameter collimator, the gamma-ray detector, and the positioning laser pointer. (b) The gamma-chopper is shown from the perspective of the laser pointer, with the electric motor visible.

various spectral hardness hitting the detector at different altitudes. This is important for the TGE and TGF search algorithm because as λ changes with altitude, the statistical significance of the detection of k events changes as well.

3.5. Artificial TGFs

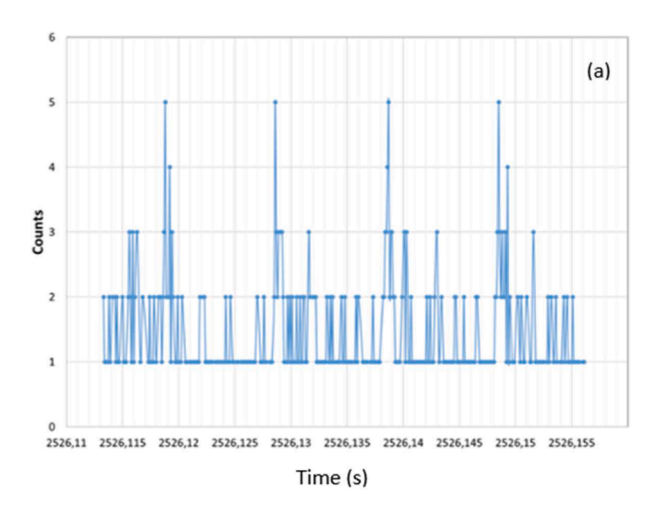
Then using the sea level gamma-ray radiation probabilities we can look at the short bursts of gamma-rays that were produced in the lab to test the TGF search algorithm. These artificial TGF pulses have durations down to $100\,\mu s$ and they enable us to better understand how the detector would respond to a natural TGF event.

A special rotary disk experimental machine (gamma-chopper) was used to generate pulses with durations of 0.1 to 1.0 ms (See Fig. 9). This experimental setup consists of a high intensity gamma source and a rotating collimator to achieve a pulsating artificial signal of the desired duration. Lab-based tests were carried out using the gamma-chopper instrument in order to simulate the short, pulsed gamma-radiation characteristic of TGFs.

We achieved an angular velocity of 3035 rpm with the rotating disk, which corresponds to 50.6 revolutions per second (rps). If we consider the fact that for a full rotation there will be two times when the rotating collimator allows the radiation to pass through, then we see that the collimator will modulate the radiation signal with a frequency of 101.2 Hz and the corresponding period is $\sim\!10$ ms. With the disk diameter of 202 mm (634 mm circumference) and the collimator hole diameter of 22 mm, the hole will be uncovered 44/634 = 7 % of the time, leading to a pulse width of 0.7 ms.

The distance from the 6 GBq Cs-137 radiation source to the detector was 1392 mm which lead to a 350 $\mu Sv/h$ dose rate pulses and the background level in the lab when the rotating collimator was not aligned with the detector was 1–3 $\mu Sv/h$. For comparison, during a transcontinental flight the passengers and crew are exposed to a dose rate of $\sim\!10~\mu Sv/h$. The signal-to-noise (signal-to-background) ratio of 100 in this experiment allows for the pulses to be clearly delineated.

In Fig. 10a we can see that the number of photons reported per 100 μs interval never goes above 5. This is due to the data acquisition system of the gamma-ray detector which cannot resolve individual photons that occur within 20 μs . Thus, within 100 μs there can be a maximum of five pulses reported (all with the same 100 μs resolution time stamp), and the energies of the photons within the 20 μs window are added up leading to the pile-up effect seen in Fig. 10.b. We can see that up to ten photons



100 2526,11 2526,115 2526,12 2526,125 2526,13 2526,135 2526,14 2526,145 2526,15 2526,155

Fig. 10. (a) The detector response to the artificial gamma-ray flash. Note that due to the data acquisition system the counts per $100~\mu s$ interval never increase above five. (b) Energy channel response during the artificial gamma-ray flash. The Cs-137 isotope emits at 662~keV which corresponds to channel 66, yet we see those channels well above 66 responded. This is due to the pileup effect that occurs when several photons are counted together during a time window that is equivalent to the response time of the detector.

Time (s)

were reabsorbed during a single time window which lead to channel read-outs near channel 500 (5200 keV) even as the characteristic source energy for the Cs-137 isotope was 662 keV.

The results show that the detector is more suited for TGE measurements, and that photon count alone is not an adequate criterion when searching for TGFs with this detector. The artificial gamma-ray flashes allowed us to better understand the spectral and temporal responses of the detector and test our TGF search methods with a view toward future ground- and aircraft-based measurements.

3.6. In-flight measurements and preliminary results

The prototype gamma-ray detector has been placed on each aircraft participating in the study. In 2020–2021, we deployed the detector on 16 commercial airline flights and 20 private flights in the Northern Hemisphere, and we plan to deploy it on Embraer test flights in the Southern Hemisphere in late 2024.

Results of this pilot study demonstrated the feasibility of using these detectors onboard both commercial and general aviation aircraft. The detector radiation safety certification was obtained, data acquisition

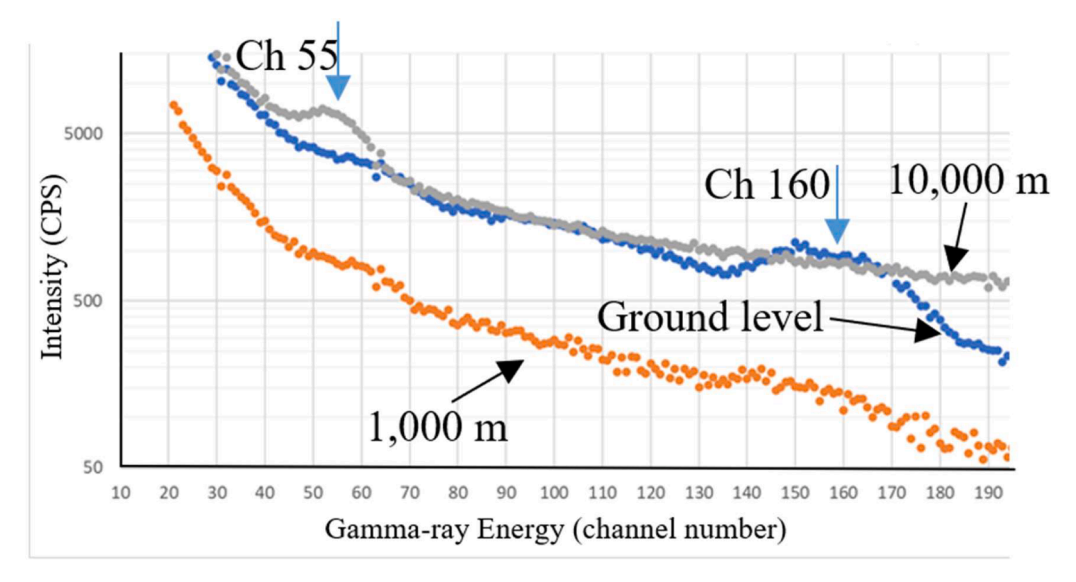


Fig. 11. The gamma-ray spectrum on the ground (blue), at 1000 m (orange), and at 10,000 m (gray). At 10,000 m a photopeak is visible near channel 55, and on the ground a photopeak is detected at channel 160.

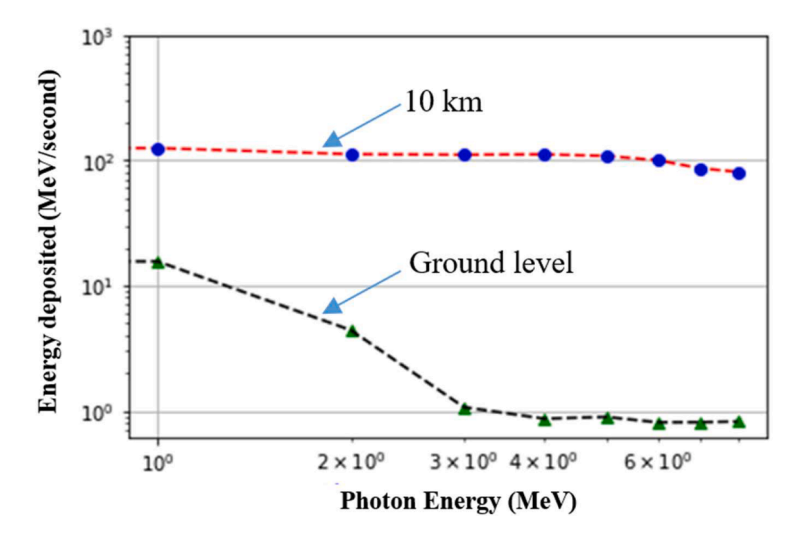


Fig. 12. Deposited energy vs. photon energy at ground level and at an altitude of 10 km. The black dashed line indicates the spectrum observed at ground level and the red dashed line indicates the spectrum at 10 km. This shows that the energy deposited per energy bin (bin size of 1 MeV) per second during airborne observations is considerably higher and has a differently shaped spectrum than at ground level. At 10 km, the energy per bin only slowly decreases with increasing photon energy.

protocols were developed, GPS signal and power requirements were tested in-flight, and feedback from the flight crew was documented. Thus, the pilot study enables a more seamless implementation of a larger-scale study.

Throughout the aircraft-based measurement campaign, we measured the spectrum of the incoming gamma-radiation at various altitudes. Similar to the total gamma-ray flux data, the spectrum also varies with altitude, thus it is interesting to analyze not only the overall intensity variations, but also the changes in count per second (CPS) values at specific energy levels. This allows one to understand the measured data and apply energy dependent baseline radiation levels when calculating the Poisson distributions needed to determine the statistical significance of TGF and TGE events.

We analyzed the spectra at three altitudes, (0 m, 1000 m, and 10,000 m) under fair-weather conditions, and they are shown in Fig. 11.

We can see that the radiation values measured at $1000\,\mathrm{m}$ are lower throughout the spectrum than those measured at $10,000\,\mathrm{m}$, and they are also lower than the ground-based measurements. The radon radiation from the ground is diminished at $1000\,\mathrm{m}$, yet radiation of cosmic origin

is not yet increased in a significant way, so the flights conducted with general aviation aircraft revealed the lowest radiation levels.

It is worth noting the photopeaks near channel 55 for the commercial aircraft-based measurements (10,000 m), and near channel 160 for the ground-based detection (see Fig. 11). Channel 55 corresponds to an energy of 500 keV with a measurement uncertainty of ± 20 keV, and channel 160 corresponds to a gamma-ray energy of 1480 keV with a measurement uncertainty of ± 20 keV. Potassium-40 has an emission line at 1460 keV. This isotope is known to contribute to the groundbased background radiation, so it is likely that the photopeak near channel 160 is due to Potassium-40. The strong photopeak near channel 55 is most likely due to electron-positron annihilation which emits the well-known 511 keV line. This observation amounts to the detection of antimatter (positrons) in the atmosphere under fair-weather conditions. It is important to understand how the detector behaves during flight both for the efficient operation of the hardware and to measure the baseline radiation level that we expect at various altitudes (see Figs. 12 and 13).

General Aviation (GA), the term used to refer to non-commercial air

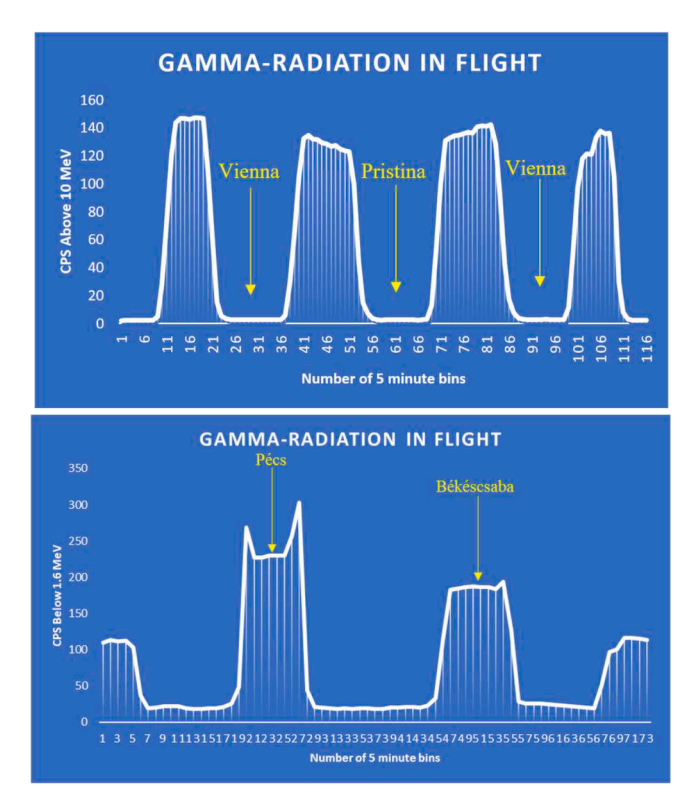


Fig. 13. (a) Radiation measurements conducted in-flight onboard a commercial aircraft during an about 10-hour long round trip. The CPS above the 10 MeV level increased from 2 to around 150 as the plane reached its cruising altitude of 10,000 m. (b) Radiation measurements conducted in-flight onboard a GA aircraft with a cruising altitude of 1000 m during a route which lasted for a total of 6 h. CPS below 1.6 MeV is shown. A comparison of panel a with panel b confirms that low energy radiation is dominated by ground sources while high energy radiation is dominated by cosmic sources.

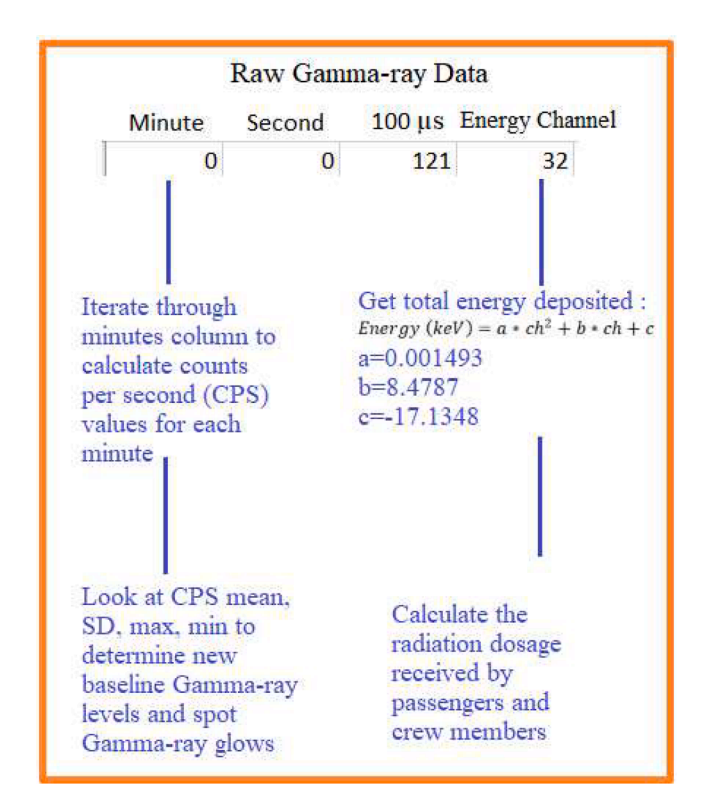


Fig. 14. Interpretation of raw gamma-ray data from Dr. Enoto's detector.

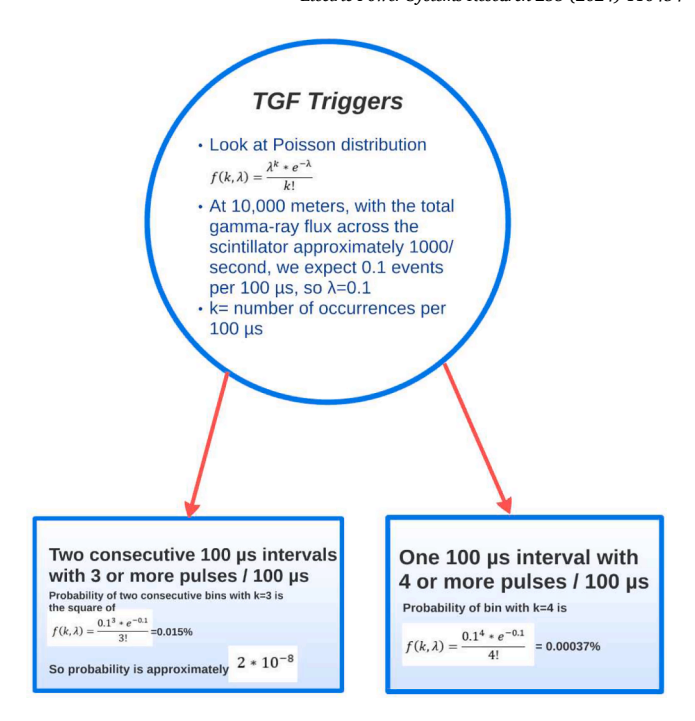


Fig. 15. Search for TGF triggers using raw gamma-ray data from Dr. Enoto's detector.

transport aircraft, represent more than 90 % of the 210,000 aircraft registered in the US [39], so it is important to explore ways to understand how energetic radiation can affect GA. Measurements have been conducted using GA aircraft during the Summer of 2021 in Hungary with the purpose of developing a testing protocol and conducting measurements. The GA flights in this study were conducted using a Cessna 172 airplane which flew at Flight Level 30 (~1000 m). The radiation intensity values for general aviation flights are shown in Fig. 14.

The CPS below the 1.6 MeV level changed from (1) 110 CPS in Jakabszállás to (2) 20 CPS in-flight to (3) 230 CPS in Pécs to (4) 19 CPS in-flight to (5) 185 CPS in Békéscsaba to (6) 22 CPS in-flight to (7) 115 as the plane reached its destination in Jakabszállás. It is interesting to note that the CPS at this energy level in-flight at 1000 m is up to an order of magnitude lower than the radiation level measured at ground level. As primordial radionuclides - such as uranium and thorium found in the ground, soil, and water - decay they produce decay products such as radon and thoron which contribute to terrestrial radiation. As the airplane takes off, its distance from the terrestrial radiation sources increases and the intensity of the radiation in this energy range (which is due to terrestrial sources) decreases. This is visible in Fig. 11, and it also shows spikes during the landing and takeoff at Pécs airport. There are uranium mines near Pécs, and its soil is rich in uranium, so it is possible that during the takeoff and landing pattern the airplane overflew such uranium-rich soils.

At an altitude of 1000 m the increase in cosmic radiation is still less than a factor of two, as shown in Fig. 15. This means that unlike commercial airline flights, general aviation flights with cruising altitudes close to 1000 m, do not experience a significant increase in radiation doses as CPS values at lower energies due to terrestrial sources being suppressed (see Fig. 14) and the higher energy radiation intensity only increases marginally (see Fig. 15).

3.7. Thunderstorm ground enhancement (TGE) search

Measurements of gamma-ray glows have been conducted in clouds (e.g. Eack et al. 1996a, 1996b, 2000) as well as on the ground (Chilingarian et al. 2010,2011; Wada et al., 2019). These generally last for tens of seconds or more and represent an enhancement of up to one to

two orders of magnitude in the gamma-ray levels. They are not associated with lightning processes, but they are due to runaway electrons accelerated toward ground in the high-field regions of the thundercloud. Lightning can terminate TGEs (Chilingarian et al. 2010, 2011, 2017, 2020).

We developed a TGE search algorithm which plots and detects TGE events and separates them from background noise. Fig. 16 outlines how we interpret the raw data from Dr. Enoto's gamma-ray detector, and how we calculate radiation doses.

3.8. Terrestrial gamma-ray flash (TGF) search

As shown in Fig. 17, we developed a TGF search algorithm to locate possible TGF events within the gamma-ray dataset. This approach considers the 100 μs timing bins of the detector and the statistical probability of false positives.

4. Discussion and summary

Lightning related energetic radiation has traditionally been measured from satellites or from the ground. Here we present new measurement, calibration, and detection approaches with the aim of better understanding the energetic radiation emitted from lightning and thunderclouds. Both commercial and general-aviation aircraft travel at different cruising altitudes, creating different radiation environments for passengers and crew members. The lab-based measurements allowed us to verify the spectral and temporal response of the prototype gammaray detector. Extensive calibration measurements were conducted using eight different radioactive isotopes to test the detector photopeak response. Dynamic track measurements were performed to test how the detector responds to both slow and fast impulses, and high-intensity sources were used to test detector response when it is saturated. We found that the detector had a photopeak measurement uncertainty of ± 20 keV, and that it had a memory overflow problem when it reached saturation. We also measured the directionality of the detector, which is essential for the interpretation of aircraft-based measurements, as radiation can be coming from all 3 dimensions in this case. In the lab we were able to test both the temporal response of the detector and the detection algorithm by creating artificial Terrestrial Gamma-ray Flashes (TGFs) and artificial Thunderstorm Ground Enhancements (TGEs).

Both TGF and TGE search algorithms were developed and tested using airplane-based measurements during fair-weather conditions (i.e. the aircraft did not encounter thunderclouds nor did it fly near them) over a total of 180 h. Both general aviation flights (with characteristic cruise altitudes of 1000 m) and commercial flights (with characteristic cruise altitudes of 10,000 m) were conducted. We can see that the radiation profiles at sea level, 1000 m, and 10,000 m are very different. We observed signatures of the 511 keV positron-electron annihilation line in the 10-km altitude measurements and identified the Potassium-40 emissions in the ground-based records. These initial aircraft-based measurements will enable larger-scale and more comprehensive studies in the future.

CRediT authorship contribution statement

Istvan Kereszy: Conceptualization, Data curation, Formal analysis, Investigation, Methodology, Project administration, Visualization, Writing – original draft, Writing – review & editing. Vladimir A. Rakov: Methodology, Project administration, Supervision, Writing – original draft, Writing – review & editing. Attila Gulyas: Data curation, Investigation, Methodology, Resources, Software. Ziqin Ding: Investigation, Methodology, Resources. Teruaki Enoto: Conceptualization, Data curation, Resources, Software. Yuuki Wada: Data curation, Methodology, Resources, Software. Listz Araújo: Investigation, Writing – review & editing. Miguel Guimarães: Investigation, Writing – review & editing.

Declaration of competing interest

The authors declare that they have no known competing financial interests or personal relationships that could have appeared to influence the work reported in this paper.

Data availability

Data will be made available on request.

Acknowledgements

This work was supported in part by NSF grant AGS-2114471.

References

- I. Kereszy, V.A. Rakov, Z. Ding, J.R. Dwyer, Ground-based observation of a tgf occurring between opposite polarity strokes of a bipolar cloud-to-ground lightning flash, J. Geophys. Res. Atmos. 127 (9) (2022) e2021JD036130.
- [2] Y. Wada, T. Enoto, Y. Nakamura, Y. Furuta, T. Yuasa, K. Nakazawa, T. Morimoto, M. Sato, T. Matsumoto, D. Yonetoku, et al., Gamma-ray glow preceding downward terrestrial gamma-ray flash, Commun. Phys. 2 (1) (2019) 67.
- [3] J.R. Dwyer, M.M. Schaal, E. Cramer, S. Arabshahi, N. Liu, H.K. Rassoul, J.D. Hill, D. M. Jordan, M.A. Uman, Observation of a gamma-ray flash at ground level in association with a cloud-to-ground lightning return stroke, J. Geophys. Res. Space Phys. 117 (A10) (2012).
- [4] A. Chilingarian, A. Daryan, K. Arakelyan, A. Hovhannisyan, B. Mailyan, L. Melkumyan, G. Hovsepyan, S. Chilingaryan, A. Reymers, L. Vanyan, Ground-based observations of thunderstorm-correlated fluxes of high-energy electrons, gamma rays, and neutrons, Phys. Rev. D 82 (4) (2010) 043009.
- [5] A. Chilingarian, G. Hovsepyan, A. Hovhannisyan, Particle bursts from thunderclouds: natural particle accelerators above our heads, Phys. Rev. D 83 (6) (2011) 062001.
- [6] A. Chilingarian, G. Hovsepyan, L. Kozliner, Extensive air showers, lightning, and thunderstorm ground enhancements, Astropart. Phys. 82 (2016) 21–35.
- [7] A. Chilingarian, Y. Khanikyants, E. Mareev, D. Pokhsraryan, V.A. Rakov, S. Soghomonyan, Types of lightning discharges that abruptly terminate enhanced fluxes of energetic radiation and particles observed at ground level, J. Geophys. Res. Atmos. 122 (14) (2017) 7582–7599.
- [8] A. Chilingarian, Y. Khanikyants, V.A. Rakov, S. Soghomonyan, Termination of thunderstorm-related bursts of energetic radiation and particles by inverted intracloud and hybrid lightning discharges, Atmos. Res. 233 (2020) 104713.
- [9] G.J. Fishman, P.N. Bhat, R. Mallozzi, J.M. Horack, T. Koshut, C. Kouveliotou, G.N. Pendleton, C.A. Meegan, R.B. Wilson, and W.S. Paciesas. Discovery of intense gamma-ray flashes of atmospheric origin. 1994.
- [10] N. Østgaard, T. Gjesteland, J. Stadsnes, P.H. Connell, B. Carlson, Production altitude and time delays of the terrestrial gamma flashes: revisiting the burst and transient source experiment spectra, J. Geophys. Res. Space Phys. 113 (A2) (2008).
- [11] R.P. Lin, B.R. Dennis, G.J. Hurford, D.M. Smith, A. Zehnder, P.R. Harvey, D.W. Curtis, D. Pankow, P. Turin, M. Bester, et al. The reuven ramaty high-energy solar spectroscopic imager (rhessi). The Reuven Ramaty High-Energy Solar Spectroscopic Imager (RHESSI) mission description and early results, pages 3–32, 2002.
- [12] D.M. Smith, L.I. Lopez, R.P. Lin, C.P. Barrington-Leigh, Terrestrial gamma-ray flashes observed up to 20 mev, Science 307 (5712) (2005) 1085–1088.
- [13] M.S. Briggs, G.J. Fishman, V. Connaughton, P.N. Bhat, W.S. Paciesas, R.D. Preece, C. Wilson-Hodge, V.L. Chaplin, R.M. Kippen, A. Von Kienlin, et al., First results on terrestrial gamma ray flashes from the fermi gamma-ray burst monitor, J. Geophys. Res. Space Phys. 115 (A7) (2010).
- [14] S. Foley, G. Fitzpatrick, M.S. Briggs, V. Connaughton, D. Tierney, S. McBreen, J. R. Dwyer, V.L. Chaplin, P. Narayana Bhat, D. Byrne, et al., Pulse properties of terrestrial gamma-ray flashes detected by the fermi gamma-ray burst monitor, J. Geophys. Res. Space Phys. 119 (7) (2014) 5931–5942.
- [15] G.J. Fishman, M.S. Briggs, V. Connaughton, P.N. Bhat, W.S. Paciesas, A. von Kienlin, C. Wilson-Hodge, R.M. Kippen, R. Preece, C.A. Meegan, et al., Temporal properties of the terrestrial gamma-ray flashes from the gamma-ray burst monitor on the fermi observatory, J. Geophys. Res. Space Phys. 116 (A7) (2011).
- [16] C. Maiorana, M. Marisaldi, A. Lindanger, N. Østgaard, A. Ursi, D. Sarria, M. Galli, C. Labanti, M. Tavani, C. Pittori, et al., The 3rd agile terrestrial gamma-ray flashes catalog. part ii: optimized selection criteria and characteristics of the new sample, J. Geophys. Res. Atmos. 125 (11) (2020) e2019JD031986.
- [17] F. Fuschino, M. Marisaldi, C. Labanti, G. Barbiellini, E. Del Monte, A. Bulgarelli, M. Trifoglio, F. Gianotti, M. Galli, A. Argan, et al., High spatial resolution correlation of agile tgfs and global lightning activity above the equatorial belt, Geophys. Res. Lett. 38 (14) (2011).
- [18] A. Lindanger, M. Marisaldi, C. Maiorana, D. Sarria, K. Albrechtsen, N. Østgaard, M. Galli, A. Ursi, C. Labanti, M. Tavani, et al., The 3rd agile terrestrial gamma ray flash catalog. part i: association to lightning sferics, J. Geophys. Res. Atmos. 125 (11) (2020) e2019JD031985.

- [19] J.R. Dwyer, D.M. Smith, S.A. Cummer, High-energy atmospheric physics: terrestrial gamma-ray flashes and related phenomena, Space Sci. Rev. 173 (2012) 133-106
- [20] M. Tavani, A. Argan, A. Paccagnella, A. Pesoli, F. Palma, S. Gerardin, M. Bagatin, A. Trois, P. Picozza, P. Benvenuti, et al., Possible effects on avionics induced by terrestrial gamma-ray flashes, Nat. Hazards Earth Syst. Sci. 13 (4) (2013) 1127–1133.
- [21] K.D. Stephan, M.L. Shmatov, Hazards to aircraft crews, passengers, and equipment from thunderstorm-generated X-rays and gamma-rays, Radiation 1 (3) (2021) 162–173.
- [22] M.M. Meier, K. Copeland, K.E.J. Klöble, D. Matthiä, M.C. Plettenberg, K. Schennetten, M. Wirtz, C.E. Hellweg, Radiation in the atmosphere–a hazard to aviation safety? Atmosphere 11 (12) (2020) 1358.
- [23] K.B. Eack, W.H. Beasley, W. David Rust, T.C. Marshall, M. Stolzenburg, Initial results from simultaneous observation of x-rays and electric fields in a thunderstorm, J. Geophys. Res. Atmos. 101 (D23) (1996) 29637–29640.
- [24] K.B. Eack, W.H. Beasley, W. David Rust, T.C. Marshall, M. Stolzenburg, X-ray pulses observed above a mesoscale convective system, Geophys. Res. Lett. 23 (21) (1996) 2915–2918.
- [25] K.B. Eack, D.M. Suszcynsky, W.H. Beasley, R. Roussel-Dupre, E. Symbalisty, Gamma-ray emissions observed in a thunderstorm anvil, Geophys. Res. Lett. 27 (2) (2000) 185–188
- [26] P. Kochkin, A.P.J. van Deursen, M. Marisaldi, A. Ursi, A.I. De Boer, M. Bardet, C. Allasia, J.-F. Boissin, F. Flourens, N. Østgaard, In-flight observation of gamma ray glows by ildas, J. Geophys. Res. Atmos. 122 (23) (2017) 12–801.
- [27] P. Kochkin, D. Sarria, C. Skeie, A.P.J.V. Deursen, A.I. de Boer, M. Bardet, C. Allasia, F. Flourens, N. Østgaard, In-flight observation of positron annihilation by ildas, J. Geophys. Res. Atmos. 123 (15) (2018) 8074–8090.
- [28] D.M. Smith, J.R. Dwyer, B.J. Hazelton, B.W. Grefenstette, G.F.M. Martinez-McKinney, Z.Y. Zhang, A.W. Lowell, N.A. Kelley, M.E. Splitt, S.M. Lazarus, et al., The rarity of terrestrial gamma-ray flashes, Geophys. Res. Lett. 38 (8) (2011).
- [29] D.M. Smith, J.R. Dwyer, B.J. Hazelton, B.W. Grefenstette, G.F.M. Martinez-McKinney, Z.Y. Zhang, A.W. Lowell, N.A. Kelley, M.E. Splitt, S.M. Lazarus, et al.,

- A terrestrial gamma ray flash observed from an aircraft, J. Geophys. Res. Atmos. 116 (D20) (2011).
- [30] J.R. Dwyer, D.M. Smith, M.A. Uman, Z. Saleh, B. Grefenstette, B. Hazelton, H. K. Rassoul, Estimation of the fluence of high-energy electron bursts produced by thunderclouds and the resulting radiation doses received in aircraft, J. Geophys. Res. Atmos. 115 (D9) (2010).
- [31] G.S. Bowers, D.M. Smith, G.F. Martinez-McKinney, M. Kamogawa, S.A. Cummer, J. R. Dwyer, D. Wang, M. Stock, Z. Kawasaki, Gamma ray signatures of neutrons from a terrestrial gamma ray flash, Geophys. Res. Lett. 44 (19) (2017) 10–063.
- [32] T. Antoni, W.D. Apel, F. Badea, K. Bekk, A. Bercuci, H. Blümer, H. Bozdog, I. M. Brancus, C. Büttner, A. Chilingarian, et al., The primary proton spectrum of cosmic rays 5 measured with single hadrons at ground level, Astrophys. J. 612 (2) (2004) 914.
- [33] B. Bartoli, P. Bernardini, X.J. Bi, Z. Cao, S. Catalanotti, S.Z. Chen, T.L. Chen, S. W. Cui, B.Z. Dai, A. D'Amone, et al., Galactic cosmic-ray anisotropy in the northern hemisphere from the argo-ybj experiment during 2008–2012, Astrophys. J. 861 (2) (2018) 93.
- [34] R. Schlickeiser, J. Oppotsch, M. Zhang, N.V. Pogorelov, On the anisotropy of galactic cosmic rays, Astrophys. J. 879 (1) (2019) 29.
- [35] S. Mallick, V.A. Rakov, J.R. Dwyer, A study of x-ray emissions from thunderstorms with emphasis on subsequent strokes in natural lightning, J. Geophys. Res. Atmos. 117 (D16) (2012).
- [36] F.A. Fisher and J.A. Plumer. Lightning protection of aircraft. Technical report, 1977.
- [37] S. Celestin, V.P. Pasko, Energy and fluxes of thermal runaway electrons produced by exponential growth of streamers during the stepping of lightning leaders and in transient luminous events, J. Geophys. Res. Space Phys. 116 (A3) (2011).
- [38] M. Urbani, J. Montanyà, O.A.V. Velde, J.A. López, M. Arcanjo, P. Fontanes, D. Romero, J.A. Roncancio, High-energy radiation from natural lightning observed in coincidence with a vhf broadband interferometer, J. Geophys. Res. Atmos. 126 (7) (2021) e2020JD033745.
- [39] AOPA Your Freedom to Fly. (2019). Aopa.org. https://www.aopa.org/.